coatings

MDPI

Article

Physical Properties of Fe_3Si Films Coated through Facing Targets Sputtering after Microwave Plasma Treatment

Nattakorn Borwornpornmetee [1], Peerasil Charoenyuenyao [1], Rawiwan Chaleawpong [1], Boonchoat Paosawatyanyong [2], Rungrueang Phatthanakun [3], Phongsaphak Sittimart [4], Kazuki Aramaki [4], Takeru Hamasaki [4], Tsuyoshi Yoshitake [4] and Nathaporn Promros [1,*]

[1] Department of Physics, Faculty of Science, King Mongkut's Institute of Technology Ladkrabang, Bangkok 10520, Thailand; 62605035@kmitl.ac.th (N.B.); 61605016@kmitl.ac.th (P.C.); 61605015@kmitl.ac.th (R.C.)
[2] Department of Physics, Faculty of Science, Chulalongkorn University, Bangkok 10330, Thailand; paosawat@sc.chula.ac.th
[3] Synchrotron Light Research Institute, Nakhon Ratchasima 30000, Thailand; rungrueang@slri.or.th
[4] Department of Applied Science for Electronics and Materials, Kyushu University, Kasuga, Fukuoka 816-8580, Japan; phongsaphak_sittimart@kyudai.jp (P.S.); kazuki_aramaki@kyudai.jp (K.A.); takeru_hamasaki@kyudai.jp (T.H.); tsuyoshi_yoshitake@kyudai.jp (T.Y.)
* Correspondence: nathaporn_promros@kyudai.jp; Tel.: +66-86-379-8648

Abstract: Fe_3Si films are deposited onto the Si(111) wafer using sputtering with parallel facing targets. Surface modification of the deposited Fe_3Si film is conducted by using a microwave plasma treatment under an Ar atmosphere at different powers of 50, 100 and, 150 W. After the Ar plasma treatment, the crystallinity of the coated Fe_3Si films is enhanced, in which the orientation peaks, including (220), (222), (400), and (422) of the Fe_3Si are sharpened. The extinction rule suggests that the B_2–Fe_3Si crystallites are the film's dominant composition. The stoichiometry of the Fe_3Si surfaces is marginally changed after the treatment. An increase in microwave power damages the surface of the Fe_3Si films, resulting in the generation of small pinholes. The roughness of the Fe_3Si films after being treated at 150 W is insignificantly increased compared to the untreated films. The untreated Fe_3Si films have a hydrophobic surface with an average contact angle of 101.70°. After treatment at 150 W, it turns into a hydrophilic surface with an average contact angle of 67.05° because of the reduction in the hydrophobic carbon group and the increase in the hydrophilic oxide group. The hardness of the untreated Fe_3Si is ~9.39 GPa, which is kept at a similar level throughout each treatment power.

Keywords: Fe_3Si film; facing targets sputtering; wettability; mechanical property; plasma treatment

Citation: Borwornpornmetee, N.; Charoenyuenyao, P.; Chaleawpong, R.; Paosawatyanyong, B.; Phatthanakun, R.; Sittimart, P.; Aramaki, K.; Hamasaki, T.; Yoshitake, T.; Promros, N. Physical Properties of Fe_3Si Films Coated through Facing Targets Sputtering after Microwave Plasma Treatment. *Coatings* **2021**, *11*, 923. https://doi.org/10.3390/coatings11080923

Academic Editor: Rafal Chodun

Received: 22 June 2021
Accepted: 26 July 2021
Published: 1 August 2021

1. Introduction

There are a variety of materials that could pair with silicon (Si) to form a silicide composite such as nickel, titanium, chromium, and iron (Fe) to name a few [1]. Among those elements, Fe is an excellent element to merge with Si because both are abundant within the earth [2,3]. Iron silicide (FeSi) possesses various phases, ranging from the nonmagnetic metallic FeSi to the ferromagnetic iron silicide (Fe_3Si), all with unique properties and potential applications of their own [2–8]. Fe_3Si is an outstanding specimen among the phases of FeSi because Fe_3Si owns the following striking features: an almost identical lattice constant to those of gallium arsenide (GaAs) [9], a slight lattice parameter misfit of −2.5% with $FeSi_2$ owning the β phase and 4.2% with Si [4,5,9,10], an impressive set of magnetic properties of a slight coercive field of 7.5 Oe and a comparatively high spin polarization of 45%, and an impressive thermal stability of over 800 K Curie temperature [5,9,11,12]. These features make Fe_3Si attractive for the use in spin transistor application [2–8]. Aside from its magnetic properties, Fe_3Si also has good physical properties such as high hardness and respectable corrosion resistance [13]. Additionally, Fe_3Si films possess a smooth surface

that can be epitaxially produced on the (111) orientation Si wafer [5,9,10]. Hence, it also generates attention as a hard coating material.

Previously, our research group epitaxially created Fe_3Si films onto Si wafers owning a (111) orientation at ambient temperature, relying on sputtering with a facing targets system [5,14–16]. This system provides several merits such as a high plasma density, high-energy particle, stable substrate temperature, low stoichiometry discrepancy, and low plasma damage [5,14–16]. The produced Fe_3Si films also appear to be of a dominant B_2 structure for all existing basic structures (DO_3, A_2 and B_2) of Fe_3Si [5]. We also created the Fe_3Si films at different substrate temperatures, which uncovered that 300 °C is the most suitable substrate temperature for an epitaxial deposition of Fe_3Si films [4]. Employing a 300 °C substrate temperature, Fe_3Si structures are enhanced while they remained at the same phase and kept their electromagnetic traits [4]. Our prior studies on Fe_3Si mainly focused on the structural and magnetic properties of the films [4,5,9–12]. Despite those, there has been little research that involves the wetting angle and the mechanical characteristics, including the hardness and reduced elastic modulus for the Fe_3Si film surfaces.

Many researchers have reported that the physical characteristics of films can be altered via the usage of plasma treatment procedures [17–23]. Plasma treatment is a procedure that changes the material's surface, leading to a change in roughness [17–22]. Plasma ions can chemically react with the film's surface and can also physically bombard some particles or contaminant from the surface, both resulting in the modification of the surface and wetting properties, including an improvement of film surface quality [17–23]. Among the conventional plasma, argon (Ar) plasma possesses a set of intriguing characteristics [19–23]. Ar plasma treatment roughens the surface of the material and can also control surface oxidation, due to the fact that the plasma can either break the oxygen bond with the metal surface or generate an active hydroxyl group on the surface [20,21]. It has been reported that Ar plasma can shift the wetting state of materials from hydrophobic to hydrophilic [21–23]. According to literature, variation of the generating power influences the plasma properties and their interaction above the sample's surface [20,23]. C.C. Surdu-Bob et al. [20] discovered that low power plasma can induce oxidation on films, while high power plasma can sputter etch a GaAs film's surface. L. Ru and C. Jie-Rong [23] studied the effect of plasma power on the wettability of poly-vinyl chloride (PVC). The PVC samples were originally hydrophobic, but the wetting state shifted to hydrophilic after Ar plasma treatment. The hydrophilicity of the treated PVC increased correspondingly to the raising of plasma power. Hence, Ar plasma treatment with power variations should have a potential for the surface modification of Fe_3Si films.

For these reasons, this research work focuses on the modifications of the roughness and chemical composition over the Fe_3Si film's surface through Ar plasma treatment under various powers, to change the wettability and the mechanical properties of the Fe_3Si films. The wetting and mechanical properties for Fe_3Si films are provided, including the effect of microwave (MW) plasma treatment on such properties. Fe_3Si films were formed on Si wafer substrates via facing targets sputtering at 300 °C of substrate temperature, then, separated for Ar plasma treatment at 50 to 150 W. The effect of power on the characteristics of all Fe_3Si samples, untreated and treated, was to be examined through several characterization techniques. It was expected that the roughness and chemical composition of the Fe_3Si surface could be changed by a variation of the plasma power under an Ar ambient, which may lead to the modifications of the wetting angle and hardness. The samples in this research were investigated from a single Fe_3Si sample, while there may be a minor deviation from the results of the other Fe_3Si samples under the same experimental condition.

2. Materials and Methods

2.1. Epitaxial Creation of Fe_3Si Films

The substrate of n-type Si wafers (SUMCO Corp., Tokyo, Japan) (orientation: (111), resistivity: 1000–4000 ohm·cm) was used to produce the Fe_3Si films. The Si wafer cleaning was performed by the usage of acetone and methanol (FUJIFILM Wako Pure Chemical Corp., Osaka, Japan) inside an ultrasonic cleaner (As One, Osaka, Japan; model US-1) to remove surface contamination. After that, the Si substrates were dipped into diluted hydrofluoric acid (1%) to remove the native oxide layer. The acid was then rinsed from the substrate surface by using deionized water. Later, the cleansed Si wafers were dried by using nitrogen gas (Iwatani Corp., Osaka, Japan; 99.999% purity) and transferred to a substrate holder in the vacuum chamber.

For the sputtering systems, a couple of Fe_3Si alloy targets (TOSHIMA Manufacturing Co., Ltd., Saitama, Japan; 99.9% purity) with an atomic ratio of Fe:Si equal to 3:1 was provided as the sputtering source. The sputtering chamber was connected to a rotary pump (Alcatel Japan, Kanagawa, Japan; model CIT-Alcatel 2030C) and a turbo molecular pump (Osaka Vacuum, Osaka, Japan; model TG1003) to vacuumize the sputtering chamber. The base pressure was evacuated to below 3×10^{-5} Pa. Then, the chamber was filled with Ar gas (Iwatani Corp., Osaka, Japan; 99.9999% purity) at a constant flow rate of 15 sccm via a mass flow controller (KOFLOC, Kyoto, Japan; model 3660), where the pressure was maintained at 1.33×10^{-1} Pa. The temperature controller (OMRON, Kyoto, Japan; model E5CN) heated the Si substrate from the backside at the set temperature of 300 °C. The gas discharge was generated at a voltage of 1 kV and a current of 1.2 mA through a direct current power supply (Micro Denshi, Saitama, Japan; model HD1K-30N). The Fe_3Si films were produced at the deposition rate of 1.07 nm/min for 24 h.

Figure 1 illustrates the 2D diagram of facing targets sputtering system for the sputtering of Fe_3Si films. The circular Fe_3Si targets were provided on both facing cathodes, where the positioning of the substrate located perpendicularly to the targets and outside the ion bombardment confined to over the targets [24]. Permanent magnets were mounted beneath each cathode to control and speed up the charged particles [24]. The inert gas was introduced through the gas feed system, where the gas ions collided with the target planar at the cathode with the same negative voltage [24]. The emitted electrons from the collision were sped up by the electric and magnetic fields [24]. The electrons, which are dominated by Lorentz force, moved toward the opposite target [24]. Consequently, the ionization efficiency for facing targets sputtering could be improved, including deposition rate [24]. The sputtered atoms moved onto the heated substrate surface and condensed into the Fe_3Si films [24].

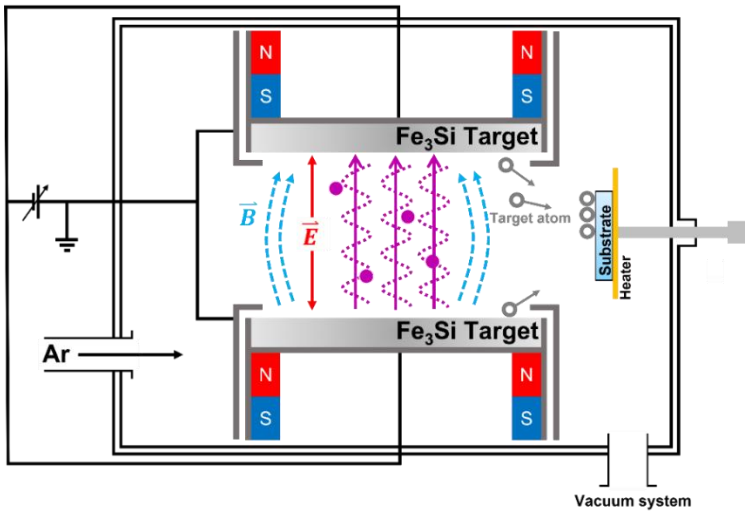

Figure 1. Schematic of facing targets sputtering apparatus used in creating Fe_3Si films.

2.2. Surface Modification of Fe_3Si Films

After the production, the Fe_3Si films were divided for surface treatment with Ar plasma using a commercial plasma system (Diener Electronic, Ebhausen, Germany; model PICO) equipped with a 2.45 GHz MW generator (Diener Electronic, Ebhausen, Germany; model MWG 1200), as can be seen in Figure 2. Before the treatment process, a rotary pump (ULVAC KIKO Inc., Miyazaki, Japan; model DIS-251) was employed to purge the air inside the chamber of the MW plasma system until the pressure became lower than 2 Pa, which was the base pressure of this arrangement. After that, Ar gas was introduced into the chamber at a 5 sccm flow rate, where the operating pressure for surface treatment was kept at 50 Pa throughout the treatment process. The magnetron head, on the top of the vacuum chamber, generated MW radiation with a consistent power, which was transferred to the chamber through a dielectric quartz window [25]. The channel MW radiation induced Ar gas ionization within the vacuum chamber, causing the generation of Ar plasma that bombarded the film's surface [25]. For the treatment condition, the Fe_3Si films were treated for 10 min under the various generating powers of 50, 100, and 150 W. After the process ended, the gas feed was stopped followed by a ventilation process until there was no processing gas remaining and the pressure within vacuum chamber returned to atmospheric pressure. Afterward, the treated samples were safe to be retrieved from the chamber.

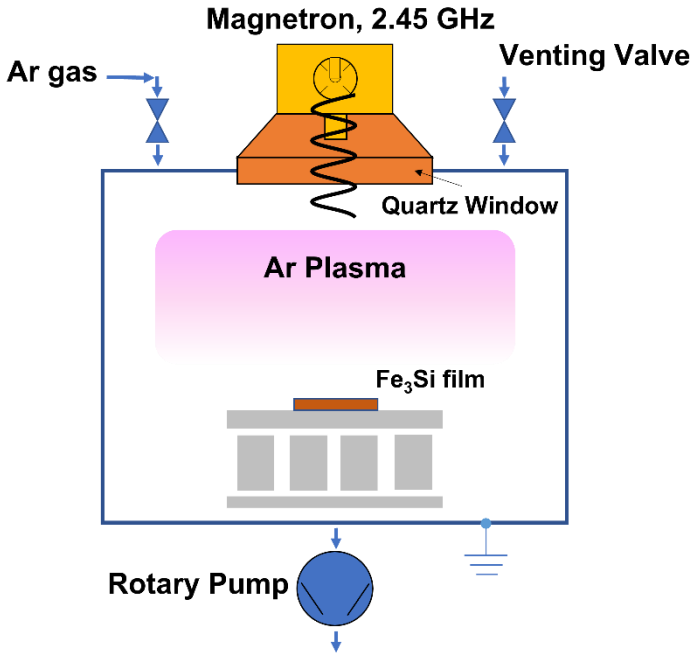

Figure 2. Arrangement of the MW plasma system.

2.3. Investigation of the Properties of Fe_3Si Films

Several properties of the untreated and treated Fe_3Si films were inspected with instruments such as X-ray diffractometer (XRD), X-ray photoelectron spectroscopy (XPS), field emission scanning electron microscope (FESEM), atomic force microscope (AFM), contact angle meter, and nanoindenter. A structural investigation of the untreated and treated Fe_3Si films, such as crystal orientation and crystallite size, was performed through XRD (Rigaku, Tokyo, Japan; model TTRAX III) under the conventional 2θ-θ scanning mode in the range 20°–90°. The size of the crystallite was simulated by using JADE software (Materials Data, Inc., Livermore, CA, USA; version 9.7.0). The atomic concentration of untreated and Ar-treated Fe_3Si films was measured by using an XPS (Kratos Analytical, Manchester, UK; model Axis Ultra DLD) and quantified through CasaXPS software (Casa Software Ltd., Devon, UK; version 2.3.24). The morphology of the Fe_3Si film's surface, before and after

plasma treatment, was studied through FESEM (Hitachi, Tokyo, Japan; model SU 8230) at 300 kx magnification, under a 10 kV load. The cross-sectional properties for all Fe_3Si films were captured at 30 kx magnification, under a 10 kV load. The surface roughness of the untreated and Ar-treated Fe_3Si was scanned through AFM (Park Systems, Suwon, Korea; model XE-120) in the non-contact scanning mode at 5×5 μm^2 of scanning area, while the root-mean-square roughness (R_{rms}) was evaluated through Gwyddion software (General Public License). The wetting properties for all the Fe_3Si film's surfaces were exposed by a contact angle meter (DataPhysics, San Jose, CA, USA; model OCA20) applying deionized (D.I.) water as the test liquid. The mechanical characteristics of hardness and reduced elastic modulus for the untreated and treated Fe_3Si films were assessed by a nanoindenter (Bruker's Hysitron, Minneapolis, MN, USA; model Ti premier).

3. Results and Discussion

3.1. Structural Properties of Fe_3Si Films

Figure 3 presents the XRD patterns for the Fe_3Si films, created at 300 °C substrate temperature, with before and after Ar plasma treatment at different powers. The sharp diffraction pattern of the untreated Fe_3Si films exhibited the preferential orientations of $Fe_3Si(220)$, $Fe_3Si(222)$, $Fe_3Si(400)$, and $Fe_3Si(422)$ at the positions of 44.42°, 56.26°, 64.70°, and 81.88°, respectively. The plasma-treated Fe_3Si films were also observed for the peaks of $Fe_3Si(220)$, $Fe_3Si(222)$, $Fe_3Si(400)$, and $Fe_3Si(422)$. The untreated Fe_3Si films showed the sharp peaks of $Fe_3Si(220)$ and $Fe_3Si(222)$, including the weak peaks of $Fe_3Si(400)$ and $Fe_3Si(422)$. These obtained peaks are well-known as successful coatings for Fe_3Si films onto Si substrate. The preferential orientations of $Fe_3Si(220)$, $Fe_3Si(222)$, $Fe_3Si(400)$, and $Fe_3Si(422)$ were also reported and confirmed by the literature of S.I. Hirakawa et al. [14] and C.B. Tang et al. [26,27]. For the details, the orientation of $Fe_3Si(222)$ denoted that the films hold a B_2 structure with a superlattice reflection of B_2–Fe_3Si crystallites [5]. The preferred orientations of $Fe_3Si(220)$, $Fe_3Si(400)$, and $Fe_3Si(422)$ showed a fundamental reflection of Fe_3Si films [5]. From the XRD peak profiling, the untreated Fe_3Si exhibited the full width at half maximum (FWHM) of the sharpest diffraction peak with a value of 0.379. After treating with 50, 100, and 150 W, the change in the FWHM was observed with the values of 0.322, 0.342, and 0.361, respectively. Based on the appraisement by Scherrer's equation through the JADE software, the crystallite size for the untreated films was around 30.925 nm. The crystallite size became 35.200, 33.175, and 31.225 nm after treating with Ar plasma at 50, 100, and 150 W, respectively. This behavior shows a rise in the crystallite size of the Fe_3Si films after the 50 W plasma treatment, which may originate from the enhancement in crystallinity of the Fe_3Si films [28–30]. The crystallinity improvement may be due to the defect annihilation progression [28]. The crystallite sizes for the Fe_3Si films treated at 100 and 150 W were both relatively smaller than that of the 50 W treated films due to orientational disarrangement caused by the more energetic ions that bombarded the surface [30,31]. In contrast, the change of grain size scarcely occurred when using Ar plasma treatment due to the nature of the noble gas, which does not cause epitaxial growth [32].

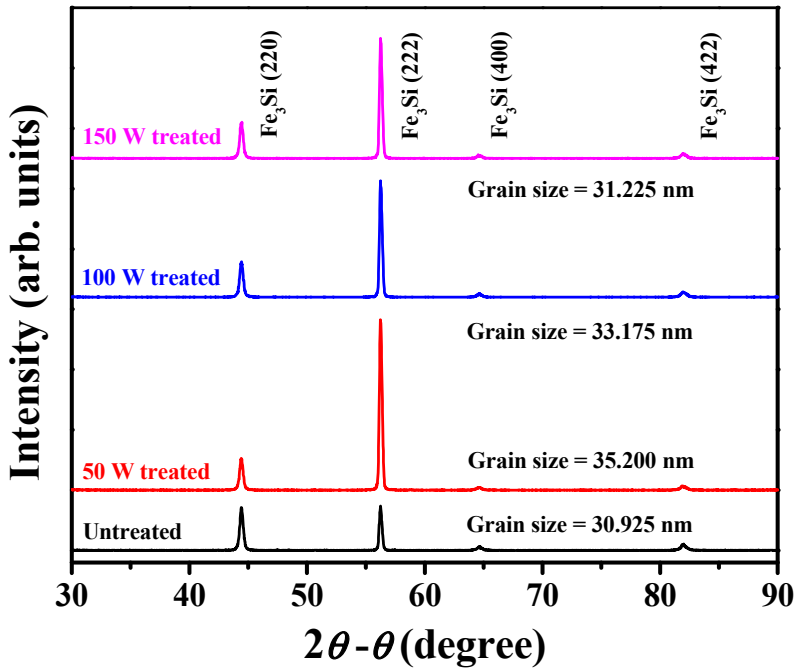

Figure 3. XRD patterns of the untreated Fe_3Si film and treated Fe_3Si films under the different powers.

3.2. Chemical Properties of Fe_3Si Films

Figure 4 demonstrates the XPS results for the surface composition of the untreated Fe_3Si films and Fe_3Si films treated at different powers. From the XPS results, the peaks of Fe 2p, O 1s, N 1s, C 1s, and Si 2p were observed. These peaks were translated into an atomic concentration of the film's surface, as represented in Table 1. The results showed an opposite behavior between the content of O 1s and C 1s concentrations for all Fe_3Si films. In response to the plasma exposure, the C 1s concentration decreased, while O 1s concentration increased as the MW power was raised. The XPS analysis revealed that, aside from Fe and Si, the surface of the Fe_3Si films also features abundant carbon and oxygen. Carbon and oxygen are common contaminants found in any material, especially on the metal-contained ones after exposing to the environmental air [33,34]. Fe_3Si is an oxidation-prone material that allows the layer of the oxide group to form on its surface easily [33]. The C 1s peak mainly originated from the layer of adventitious carbon, which forms easily on atmospherically exposed metal [34]. For N 1s, the nitrogen content may have come as a part of organic residues on the exposed surface, which is consistent with the copious amounts of C found on the surface [34]. These adventitious carbons are commonly attributed to be the reason behind hydrophobicity [22]. Under the low-pressure MW plasma treatment of Ar, high-energy ions collide with the sample surface, dissociate the organic carbon contaminants, and cause them to volatilize [22]. There is also the contribution from the oxide group, which evidently was the major contributor to hydrophilicity of the treated surface [21,22]. Hydrophilic oxide groups may come from the MW plasma chamber as the Ar gas may contain a tiny amount of oxygen, as well as the highly active groups remaining on the surface after plasma bombardment, which subsequently react with oxygen when exposed to air or plasma impurity [20,21].

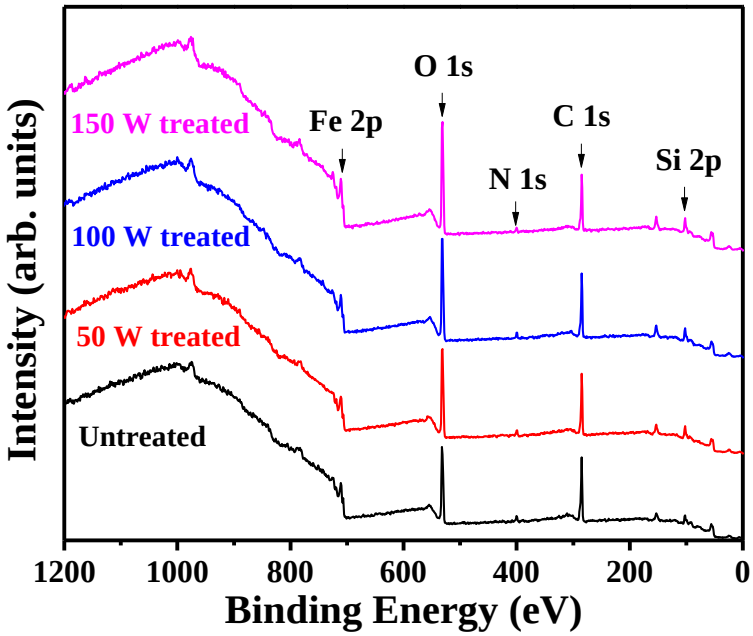

Figure 4. XPS patterns of the untreated Fe_3Si film and treated Fe_3Si films under the different powers.

Table 1. Atomic concentration of Fe_3Si films at different MW plasma treatment conditions.

Sample	Surface Atomic Concentration (at.%)				
	Fe 2p	O 1s	N 1s	C 1s	Si 2p
Untreated	10.30	47.19	3.28	35.68	3.55
Ar treated (50 W; 10 min)	12.78	53.07	2.87	26.47	4.81
Ar treated (100 W; 10 min)	13.61	56.15	2.00	23.48	4.76
Ar treated (150 W; 10 min)	15.49	56.23	2.02	20.35	5.92

3.3. Surface Morphologies of Fe_3Si Films

3.3.1. FESEM Images

Figure 5 shows typical FESEM micrographs from a top view of the untreated and treated Fe_3Si film surfaces by Ar plasma treatment under the various biased powers. These micrographs were captured at the magnification of 300 kx. Figure 5a exposes that the untreated Fe_3Si films presented an abundance of small crystallites over the entire surface area with a uniform surface structure; pinholes with a destructive surface area were not observed. This should be because of the advantages of sputtering with a pair of facing targets. Namely, this coating technique has the benefits from a low increment of substrate temperature, low-different stoichiometry films compared to the sputtering target, and high plasma density [35–37]. Additionally, the plasma's particles were detained within the generated magnetic field from the permanent magnet beneath the sputtering targets [35–37]. For a sputtering technique with facing targets, the surface of the Si wafer substrate was in parallel and situated away from the originated plasma zone during a film's coating, which led to less plasma damage over the film surface [35–37]. The surface structure of the 50 W treated Fe_3Si films was slightly changed from that of the untreated Fe_3Si films. At the higher treating powers of 100 and 150 W, the influence of the plasma treatment on the morphology of the treated Fe_3Si film's surface became more noticeable with the formation of slight bumps, including a non-smooth surface pattern and pinholes. The change of the treated Fe_3Si film's surface increased as the power was increased. This may have originated through the rise in the etching rate because of the Ar ions kinetic energy elevation [20].

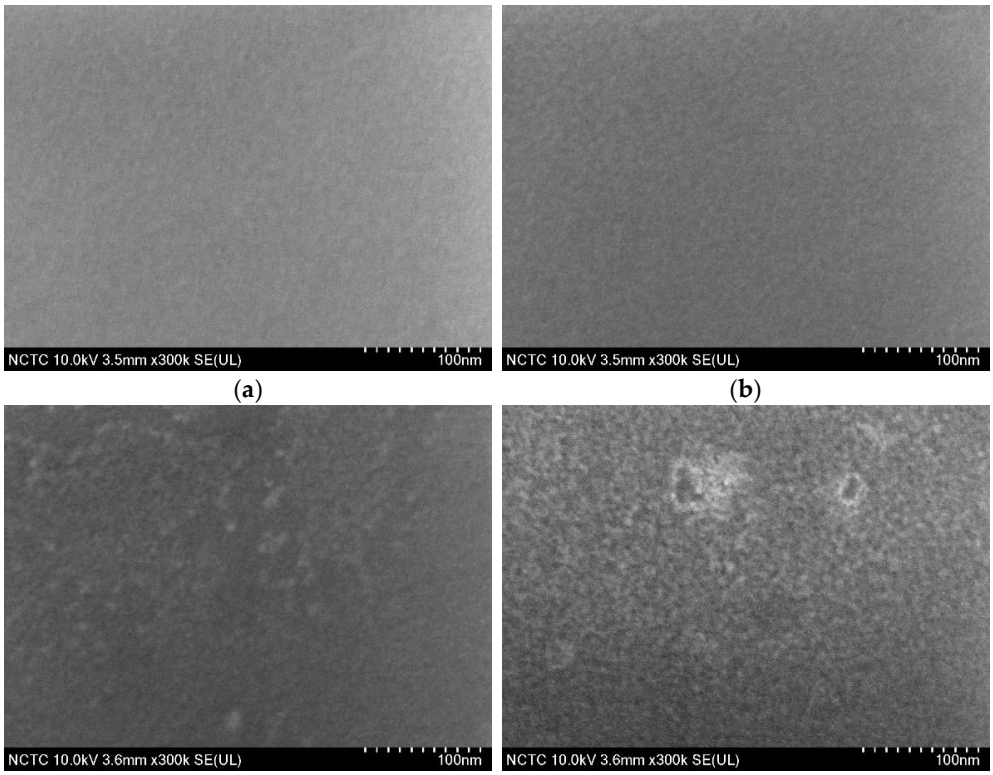

Figure 5. Planar FESEM micrographs of the coated Fe_3Si films (**a**) without and with treatment using Ar plasma at the different applied powers of (**b**) 50 W, (**c**) 100 W, and (**d**) 150 W.

Figure 6 demonstrates the representative cross-sectional FESEM micrographs of the untreated Fe_3Si films and the Fe_3Si films treated by plasma at various powers. All cross-sectional FESEM images were captured with a magnification of 30 kx. Figure 6 uncovers the linear interface between the film layer and the substrate layer. All untreated and treated Fe_3Si films were absent from deformity and discontinuity of interface between the layers. Figure 6a discloses that the constructed Fe_3Si film layer under the untreated condition owned an average thickness of 1.11 μm. The average thickness for the Fe_3Si films treated at the 50 W power was calculated to be around 1.09 μm. By raising the plasma powers to 100 and 150 W, the average thickness values of the treated Fe_3Si films slightly diminished to 1.08 and 1.05 μm, in order. The diminution of the film thickness as the power was increased may be attributable to the rise in high energetic ion bombardment, engendering a higher etching rate [20].

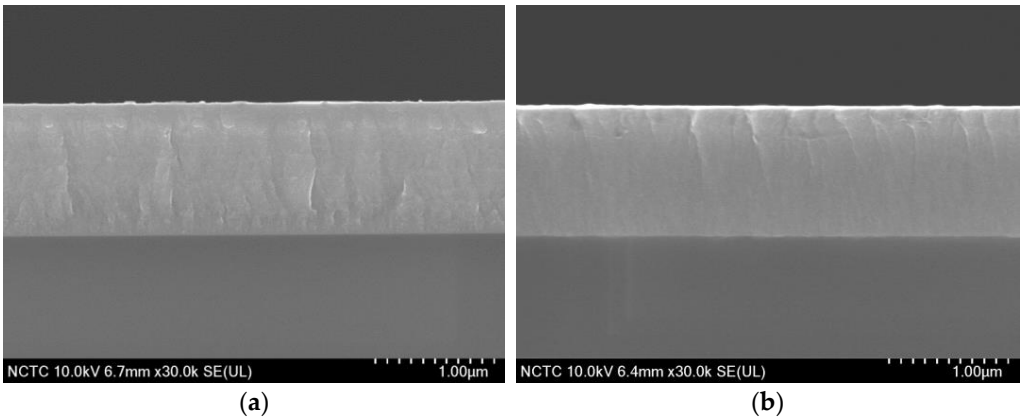

Figure 6. *Cont.*

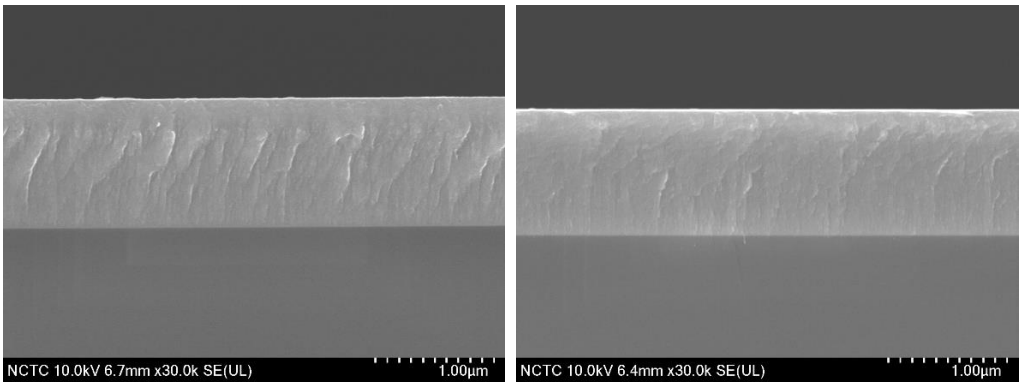

(**c**) (**d**)

Figure 6. Cross-sectional FESEM micrographs of the Fe_3Si films on Si wafers treated at different powers: (**a**) untreated and (**b**) 50 W, (**c**) 100 W, and (**d**) 150 W treated.

3.3.2. AFM Images

Figure 7 represents the AFM scanned images of the untreated and treated Fe_3Si films through Ar plasma at the different applied powers. Using AFM analysis, the determination of R_{rms} for the untreated and treated Fe_3Si film's surface could be conducted. According to the AFM topography, it was visible that the untreated Fe_3Si films exhibited a rather smooth surface with an appraised R_{rms} of 10.63 Å. This outcome was consistent with that of the FESEM result, where the smoothness of the untreated Fe_3Si films should be due to the advantages of facing targets sputtering. As a result, the damage from the plasma should have been low and generated less surface roughness over the film's surface plane [35–37]. After the treatment with Ar plasma, the R_{rms} value for the Fe_3Si films treated with 50 W power was evaluated to be 10.71 Å, where the R_{rms} value was slightly higher than that of the Fe_3Si films without plasma treatment. The treated Fe_3Si films at 100 and 150 W manifested the assessed R_{rms} values of 11.07 and 13.06 Å, respectively. Based on the surface topography, the roughness for the Fe_3Si films was not drastically changed by the Ar plasma treatment compared to similar materials such as GaAs [20]. In the process of MW plasma treatment, the Fe_3Si film surface was bombarded by highly energetic species ejecting some Fe and Si atoms from the Fe_3Si surface out, resulting in a physical change in the surface roughness [20]. There was also an occurrence of a dangling bond on the film's surface, which was not permanent as it could either diffuse from the surface or induce oxidization when aging [20,38]. It is acknowledged that elements such as Fe and Si are easily oxidized [33]. As mentioned above, there is a possibility that the Fe_3Si surface can be oxidized. Hence, its physical properties, such as the surface roughness, may have changed after the treatment. Oxidation has been proven to hardly affect the roughness of alloy surfaces, where the effect of roughness would not wear off for a considerable amount of time [39,40].

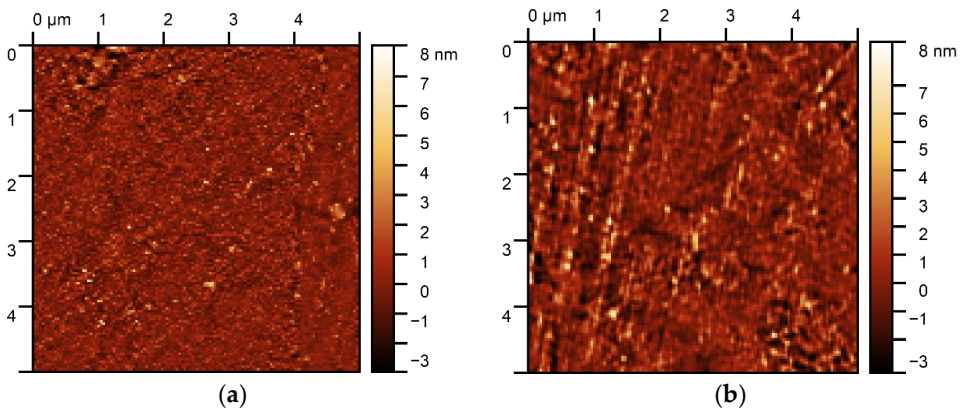

(**a**) (**b**)

Figure 7. *Cont.*

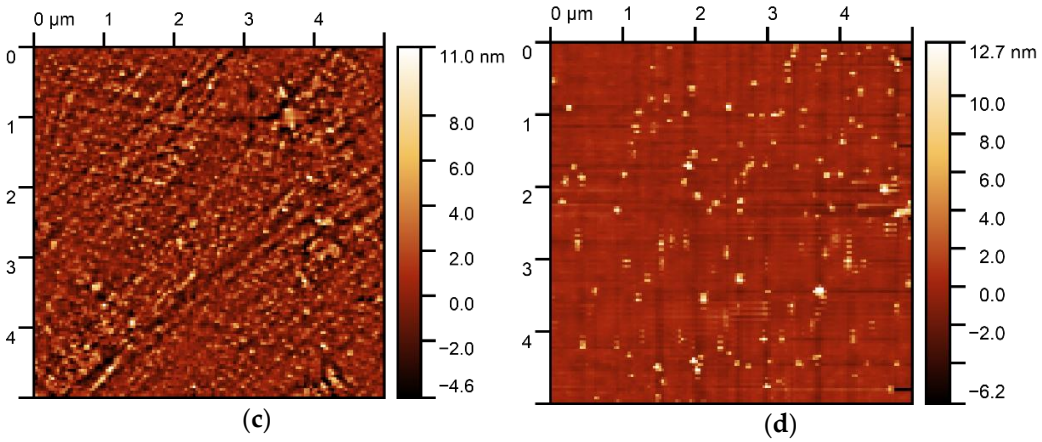

Figure 7. AFM images of the Fe_3Si film surfaces (**a**) before and after plasma treatment at (**b**) 50 W, (**c**) 100 W, and (**d**) 150 W.

3.4. Wetting Properties of Fe_3Si Films

Figure 8 displays the captured images for the contact angle measurement of the untreated and treated Fe_3Si films under the varied powers. For the surfaces of the untreated and treated Fe_3Si films, the wetting angles were determined by using D.I. water droplets. For the wetting property, it can be verified, based on the average contact angle (θ_{ca}), into super-hydrophilic ($\theta_{ca} \leq 10°$), hydrophilic ($10° < \theta_{ca} < 90°$), hydrophobic ($90° \leq \theta_{ca} < 150°$), and super-hydrophobic ($150° \leq \theta_{ca} \leq 180°$) [41]. Figure 8a represents the wetting angle between the droplet and the surface of the untreated Fe_3Si films, where the evaluated θ_{ca} was determined to be 101.7°. The result shows that the Fe_3Si films exhibited a wetting state of hydrophobic. Figure 8b–d presents the captured images between the droplet and the treated Fe_3Si films at the increased powers of 50, 100, and 150 W, respectively. After treating with Ar plasma, θ_{ca} was slightly reduced to 87.75° for the Fe_3Si films after treated at 50 W, in which the surface was determined as a hydrophilic state. At increasing powers, the θ_{ca} values for the Fe_3Si films gradually decreased to 79.20° and 67.05° at 100 W and 150 W, respectively.

It was observed that the surface of the untreated Fe_3Si films exhibited their hydrophobicity, while the surfaces of all plasma-treated Fe_3Si films turned into the hydrophilic state. The gained results of XPS revealed that more than a third of the untreated Fe_3Si film's surface was covered by the carbon functional group following by the oxide group and Fe_3Si compositional elements; the hydrophobicity for the surface should be predominantly controlled due to this reason [22]. After the plasma treatment, the XPS results for the treated films revealed a decrease of the hydrophobic carbon chemical composition by selective etching through energetic Ar ions impact [22]. Concurrently, the oxygen concentration also increased due to the highly polarized group left behind after sputter etching at low-pressure MW plasma under an Ar atmosphere [20]. These changes in surface composition resulted in the change in the wetting state from hydrophobic to hydrophilic. The trend continued as the power was increased. Based on the FESEM and AFM results, the surfaces of all the Fe_3Si films comprised nano-rough morphology. In physical terms, the surface wetting of the Fe_3Si films can be commonly attributed to the wetting models of Wenzel and Cassie-Baxter [42–45]. Wenzel and Cassie-Baxter incorporated the roughness as one of the important parameters in their models, where the former is based on surface alignment and the latter relies on the air groove [42–45]. However, our result shows a significant alteration of the wetting behavior of Fe_3Si despite the insignificant change in surface morphology. Hence, the wettability of the Fe_3Si films was predominantly dictated by their chemical composition on the surface of the untreated and plasma-treated films.

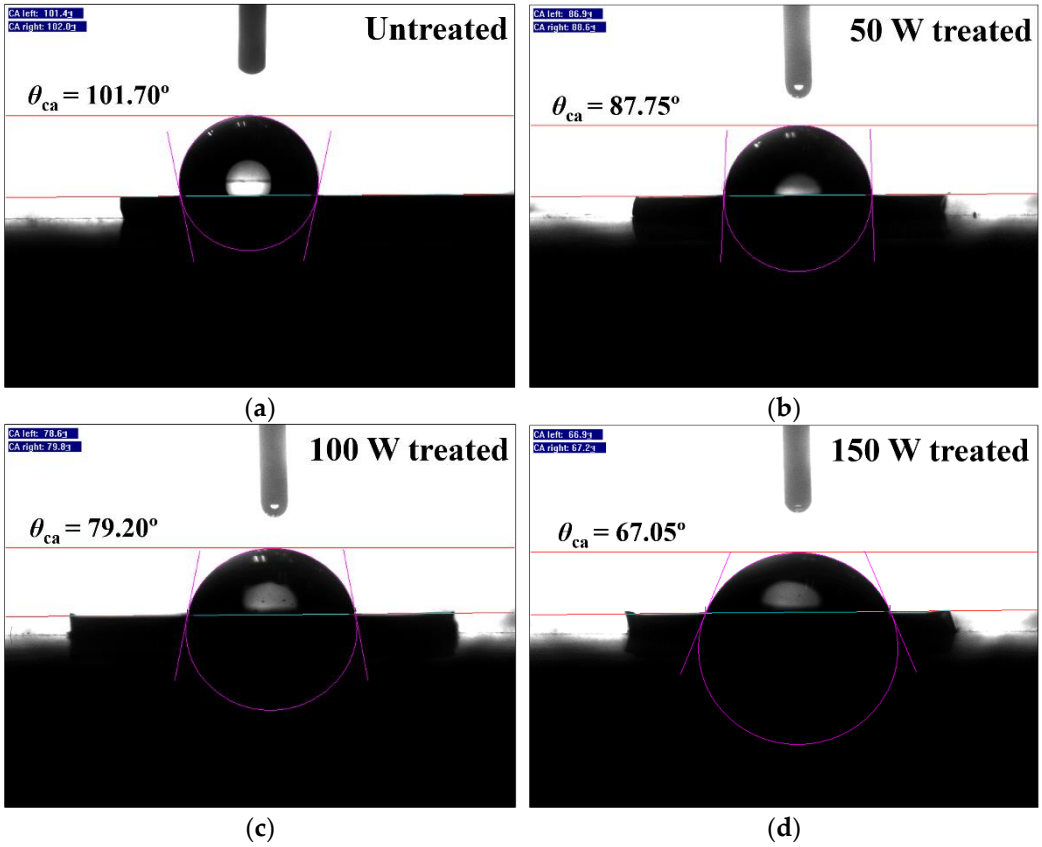

Figure 8. Images for the contact angle measurement on the surface of the Fe_3Si films (**a**) before and after treated at (**b**) 50 W, (**c**) 100 W, and (**d**) 150 W.

3.5. Mechanical Properties of Fe_3Si Films

For the mechanical properties, the nanoindentation technique using a Berkovich indenter was used to investigate the hardness and reduced elastic characteristics of the untreated and treated Fe_3Si film surfaces. The indentation test was carried on by applying an indentation load of 3 mN to all the Fe_3Si films, before and after Ar plasma treatment at 50 W–150 W. The maximum depth for the test was controlled at 10% of the thickness of all films (100 nm), where the effect of the substrate could be suppressed [46,47]. The nanoindentation test for the untreated and Ar plasma-treated Fe_3Si films was performed repeatedly, five times. Figure 9 presents the plot set of the applied indentation load versus the depth of penetration (load–depth curve) for the Fe_3Si films under the conditions of untreated, 50 W treated, 100 W treated, and 150 W treated, respectively.

The average hardness value (H) and reduced elastic modulus value (E_r) of the untreated and Ar plasma-treated Fe_3Si films were calculated from the unloading portions of their load–depth curve [48,49]. The H and E_r for all Fe_3Si samples are summarized in Table 2. Figure 10 (red line) presents the relative plot between the H for the Fe_3Si samples regarding their treatment power, with a standard deviation. The H-power plot shows the decreasing trend of the hardness characteristic of Fe_3Si films with increasing Ar plasma treatment power. In the same vein, the E_r decreases, as shown in Figure 10 (blue line), where a plot between the E_r versus power for Fe_3Si films is depicted. Based on the nanoindentation result, the H of the untreated Fe_3Si films was close to the Fe_3Si reported by various sources [25,50]. The H and E_r were almost the same, albeit slightly declined after the Ar plasma treatment. They agreed with the morphology results of the films, where the inconsistency of the film's surface was observed as the standard deviation [51]. As the plasma power increased, the deviation increasingly swayed by the accumulated plasma damage [51]. Considering the fact that the nanoindentation only penetrated 10% of the

film's thickness, these changes as a response to surface modification are insignificant when taken together.

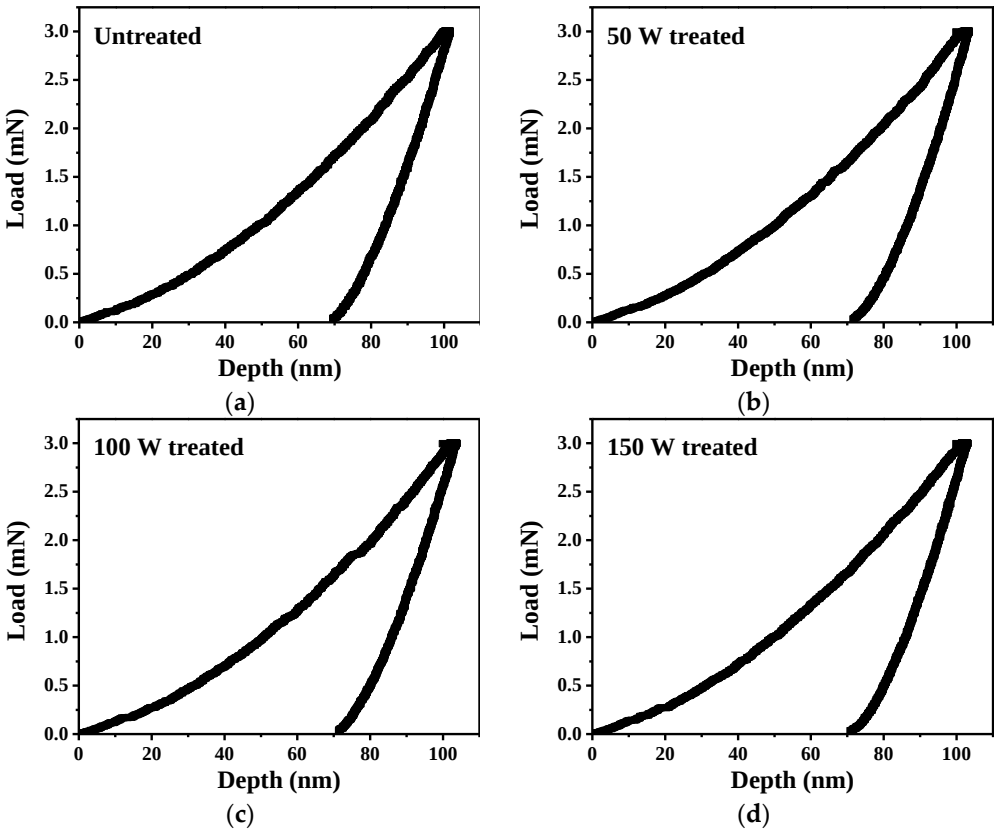

Figure 9. Load versus depth plots of the Fe_3Si films (**a**) before and after treated at (**b**) 50 W, (**c**) 100 W, and (**d**) 150 W.

Table 2. H and E_r for untreated Fe_3Si and Ar plasma-treated Fe_3Si.

Sample	H (GPa)	E_r (GPa)
Untreated	9.392 ± 0.070	204.862 ± 1.226
Ar treated (50 W; 10 min)	8.991 ± 0.069	205.943 ± 4.633
Ar treated (100 W; 10 min)	8.881 ± 0.080	208.085 ± 3.113
Ar treated (150 W; 10 min)	8.857 ± 0.094	212.693 ± 3.211

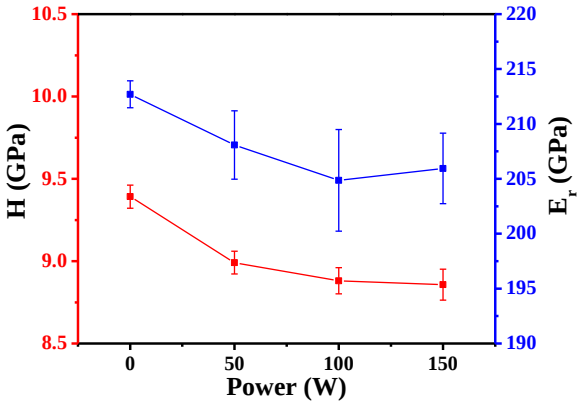

Figure 10. Plots of the (**red**) H and (**blue**) E_r with standard deviation versus plasma-treated power of the surface of the Fe_3Si films treated by Ar plasma under different powers.

4. Conclusions

The present study clarified the cause of hydrophobicity of Fe_3Si films epitaxially created through facing targets sputtering at 300 °C heated substrate and the effect of Ar plasma treatment power on the film's properties. The XRD patterns for all Fe_3Si films presented a combination of a B_2 and DO_3 Fe_3Si crystal structure. The orientational peaks of the XRD pattern became much higher at 50 W due to the suppression of surface contamination, resulting in preferable orientations. Meanwhile, the peak intensities went down as the power was increased, due to the sputter etching caused by the higher energy ions. The atomic concentration extracted from the XPS spectrum revealed that the surface of the untreated Fe_3Si was laden with carbon and oxygen, which was the general contamination. The Ar plasma treatment reduced the carbon concentration by the volatilization of the carbon atoms through ion collision. The plasma also left behind a radical reactive site which formed into an oxide layer on the Fe_3Si surface. As the power increased, the atomic concentration of oxygen also increased, while carbon decreased. The morphological outcomes, as gained from both the FESEM and AFM, showed a seamless surface with an R_{rms} of 10.63 Å for the untreated Fe_3Si films. After plasma treatment, the surface was bombarded by high energy ions, causing the appearance of pinholes which roughened the surface to 13.06 Å at 150 W of power. The film's thickness of the constructed Fe_3Si was only slightly decreased by the Ar plasma at different powers. From the contact angle results, the untreated Fe_3Si films possessed θ_{ca} of 101.7°, which changed to 67.05° after Ar plasma treatment at 150 W. The shift in hydrophobicity was likely due to the change in the chemical composition of the surface, namely, the reduction in hydrophobic organic carbon and the augmentation of the hydrophilic oxide group. The H and E_r of the untreated Fe_3Si films were not significantly influenced by the Ar plasma at different powers. For the next settlement, the effect of other plasma treatment parameters on Fe_3Si's properties such as time, pressure, and gas type can be explored. The study will mainly focus on how these parameters can affect the wettability and mechanical properties of Fe_3Si to properly determine the optimized condition for the modification of wettability and mechanical properties.

Author Contributions: Conceptualization, N.P.; methodology, N.B., P.C., R.C., R.P., P.S., K.A., T.H. and N.P.; formal analysis, N.B., P.C., R.C., P.S. and N.P.; investigation, N.B., P.C., R.C., R.P. and N.P.; writing—original draft preparation, N.B., P.C., R.C. and N.P.; writing—review and editing, N.B., P.C., R.C., B.P., P.S., T.Y. and N.P.; Visualization, N.B., P.C. and R.C.; Supervision, B.P. and T.Y. All authors have read and agreed to the published version of the manuscript.

Funding: The allowance for carrying out this research was provided by the Academic Research Fund, Faculty of Science, King Mongkut's Institute of Technology Ladkrabang, with grant numbers 2562-01-05-29, 2562-01-05-44 and 2563-02-05-36.

Institutional Review Board Statement: Not applicable.

Informed Consent Statement: Not applicable.

Data Availability Statement: The data presented in this study are available in this article.

Acknowledgments: The authors also express their gratitude for the contribution and cooperation received from Research Unit of Integrated Science for Electronic, Material and Industry (ISEMI), Faculty of Science, King Mongkut's Institute of Technology Ladkrabang.

Conflicts of Interest: The authors declare no conflict of interest.

References

1. Tam, P.L.; Cao, Y.; Nyborg, L. XRD and XPS characterisation of transition metal silicide thin films. *Surf. Sci.* **2012**, *606*, 329–336. [CrossRef]
2. Promros, N.; Yamashita, K.; Iwasaki, R.; Yoshitake, T. Effects of hydrogen passivation on near-infrared photodetection of n-type β-$FeSi_2$/p-type Si heterojunction photodiodes. *Jpn. J. Appl. Phys.* **2012**, *51*, 108006. [CrossRef]
3. Shaban, M.; Nakashima, K.; Yokoyama, W.; Yoshitake, T. Photovoltaic properties of n-type β-$FeSi_2$/p-type Si heterojunctions. *Jpn. J. Appl. Phys.* **2007**, *46*, L667. [CrossRef]

4. Nakagauchi, D.; Yoshitake, T.; Nagayama, K. Fabrication of ferromagnetic Fe_3Si thin films by pulsed laser deposition using an Fe_3Si target. *Vacuum* **2004**, *74*, 653–657. [CrossRef]
5. Yoshitake, T.; Nakagauchi, D.; Ogawa, T.; Itakura, M.; Kuwano, N.; Tomokiyo, Y.; Kajiwara, T.; Nagayama, K. Room-Temperature epitaxial growth of ferromagnetic Fe_3Si films on Si(111) by facing target direct-current sputtering. *Appl. Phys. Lett.* **2005**, *86*, 262505. [CrossRef]
6. Sittimart, P.; Duangrawa, A.; Onsee, P.; Teakchaicum, S.; Nopparuchikun, A.; Promros, N. Interface state density and series resistance of n-type nanocrystalline $FeSi_2$/p-Type Si heterojunctions formed by utilizing facing-target direct-current sputtering. *J. Nanosci. Nanotechnol.* **2018**, *18*, 1841–1846. [CrossRef]
7. Charoenyuenyao, P.; Promros, N.; Chaleawpong, R.; Saekow, B.; Porntheeraphat, S.; Yoshitake, T. Effect of annealing on surface morphology and wettability of NC-$FeSi_2$ films produced via facing-target direct-current sputtering. *J. Nanosci. Nanotechnol.* **2019**, *19*, 6834–6840. [CrossRef]
8. Mazurenko, V.V.; Shorikov, A.O.; Lukoyanov, A.V.; Kharlov, K.; Gorelov, E.; Lichtenstein, A.I.; Anisimov, V.I. Metal-insulator transitions and magnetism in correlated band insulators: FeSi and $Fe_{1-x}Co_xSi$. *Phys. Rev. B* **2010**, *81*, 125131. [CrossRef]
9. Sadoh, T.; Takeuchi, H.; Ueda, K.; Kenjo, A.; Miyao, M. Epitaxial growth of ferromagnetic silicide Fe_3Si on Si(111) substrate. *Jpn. J. Appl. Phys.* **2006**, *45*, 3598. [CrossRef]
10. Hamaya, K.; Ueda, K.; Kishi, Y.; Ando, Y.; Sadoh, T.; Miyao, M. Epitaxial ferromagnetic Fe_3Si/Si(111) structures with high-quality heterointerfaces. *Appl. Phys. Lett.* **2008**, *93*, 132117. [CrossRef]
11. Herfort, J.; Schönherr, H.P.; Ploog, K.H. Epitaxial growth of Fe_3Si/GaAs(001) hybrid structures. *Appl. Phys. Lett.* **2003**, *83*, 3912–3914. [CrossRef]
12. Lin, F.; Jiang, D.; Ma, X.; Shi, W. Structural order and magnetic properties of Fe_3Si/Si(100) heterostructures grown by pulsed-laser deposition. *Thin Solid Films* **2007**, *515*, 5353–5356. [CrossRef]
13. Schneeweiss, O.; Pizurova, N.; Jiraskova, Y.; Žák, T.; Cornut, B. Fe_3Si Surface coating on SiFe Steel. *J. Magn. Magn. Mater.* **2000**, *215*, 115–117. [CrossRef]
14. Hirakawa, S.I.; Sonoda, T.; Sakai, K.I.; Takeda, K.; Yoshitake, T. Temperature-dependent current-induced magnetization switching in $Fe_3Si/FeSi_2/Fe_3Si$ trilayered films. *Jpn. J. Appl. Phys.* **2011**, *50*, 08JD06. [CrossRef]
15. Takeda, K.; Yoshitake, T.; Nakagauchi, D.; Ogawa, T.; Hara, D.; Itakura, M.; Kuwano, N.; Tomokiyo, Y.; Kajiwara, T.; Nagayama, K. Epitaxy in $Fe_3Si/FeSi_2$ superlattices prepared by facing target direct-current sputtering at room temperture. *Jpn. J. Appl. Phys.* **2007**, *46*, 7846. [CrossRef]
16. Sakai, K.I.; Noda, Y.; Daio, T.; Tsumagari, D.; Tominaga, A.; Takeda, K.; Yoshitake, T. Current-induced magnetization switching at low current densities in current-perpendicular-to-plane structural $Fe_3Si/FeSi_2$ artificial lattices. *Jpn. J. Appl. Phys.* **2014**, *53*, 02BC15. [CrossRef]
17. Pransilp, P.; Kiatkamjornwong, S.; Bhanthumnavin, W.; Paosawatyanyong, B. Plasma Nano-modification of poly (ethylene terephthalate) fabric for pigment adhesion enhancement. *J. Nanosci. Nanotechnol.* **2012**, *12*, 481–488. [CrossRef]
18. Taweesub, K.; Visuttipitukul, P.; Tungkasmita, S.; Paosawatyanyong, B. Nitridation of Al–6%Cu alloy by rf plasma process. *Surf. Coat. Technol.* **2010**, *204*, 3091–3095. [CrossRef]
19. Berman, D.; Krim, J. Impact of oxygen and argon plasma exposure on the roughness of gold film surfaces. *Thin Solid Films* **2012**, *520*, 6201–6206. [CrossRef]
20. Surdu-Bob, C.C.; Sullivan, J.L.; Saied, S.O.; Layberry, R.; Aflori, M. Surface compositional changes in gaas subjected to argon plasma treatment. *Appl. Surf. Sci.* **2012**, *202*, 183–198. [CrossRef]
21. Prysiazhnyi, V.; Slavicek, P.; Mikmekova, E.; Klima, M. Influence of chemical precleaning on the plasma treatment efficiency of aluminum by rf plasma pencil. *Plasma Sci. Technol.* **2016**, *18*, 430–437. [CrossRef]
22. Ujino, D.; Nishizaki, H.; Higuchi, S.; Komasa, S.; Okazaki, J. Effect of plasma treatment of titanium surface on biocompatibility. *Appl. Sci.* **2019**, *9*, 2257. [CrossRef]
23. Ruand, L.; Jie-Rong, C. Studies on wettability of medical Poly (Vinyl Chloride) by remote argon plasma. *Appl. Surf. Sci.* **2006**, *252*, 5076–5082.
24. Lin, C.; Sun, D.C.; Ming, S.L.; Jiang, E.Y.; Liu, Y.G. Magnetron facing target sputtering system for fabricating single-crystal films. *Thin Solid Films* **1996**, *279*, 49–52. [CrossRef]
25. Odrobina, I.; Kúdela, J.; Kando, M. Characteristics of the planar plasma source sustained by microwave power. *Plasma Sources Sci. Technol.* **1998**, *7*, 238. [CrossRef]
26. Tang, C.B.; Wen, F.R.; Chen, H.X.; Liu, J.J.; Tao, G.Y.; Xu, N.J.; Xue, J.Q. Corrosion characteristics of Fe_3Si intermetallic coatings prepared by molten salt infiltration in sulfuric acid solution. *J. Alloys Compd.* **2019**, *778*, 972–981. [CrossRef]
27. Chang-Bin, T.; Hong-Xia, C.; Fu-Rong, W.; Ni-Jun, X.; Wei, H.; Juan-Qin, X. Facile preparation and tribological property of alloyed Fe_3Si coatings on stainless steels surface by molten-salt infiltration method. *Surf. Coat. Technol.* **2020**, *397*, 126049. [CrossRef]
28. Sattar, H.; Jielin, S.; Ran, H.; Imran, M.; Ding, W.; Gupta, P.D.; Ding, H. Impact of microstructural properties on hardness of tungsten heavy alloy evaluated by stand-off LIBS after PSI plasma irradiation. *J. Nucl. Mater.* **2020**, *540*, 152389. [CrossRef]
29. Lin, W.T.; Chen, S.H.; Chan, S.H.; Hu, S.C.; Peng, W.X.; Lu, Y.T. Crystallization phase transition in the precursors of CIGS films by Ar-ion plasma etching process. *Vacuum* **2014**, *99*, 1–6. [CrossRef]

30. Fernández, S.; Santos, J.D.; Munuera, C.; García-Hernández, M.; Naranjo, F.B. Effect of Argon Plasma-treated polyethylene terepthalate on ZnO:Al properties for flexible thin film silicon solar cells applications. *Sol. Energy Mater. Sol. Cells* **2015**, *133*, 170–179. [CrossRef]
31. Madera, R.G.B.; Martinez, M.M.; Vasquez, M.R. Effects of rf plasma treatment on spray-pyrolyzed copper oxide films on silicon substrates. *Jpn. J. Appl. Phys.* **2017**, *57*, 01AB05. [CrossRef]
32. Douglas, E.A.; Sheng, J.J.; Verley, J.C.; Carroll, M.S. Argon-Germane In Situ Plasma Clean for Reduced Temperature Ge on Si Epitaxy by High Density Plasma Chemical Vapor Deposition. *J. Vac. Sci. Technol.* **2015**, *33*, 41202. [CrossRef]
33. Chen, G.L.; Peng, J.H.; Xu, W.X. Surface reaction of polycrystalline Fe_3Si alloys with oxygen and water vapor. *Intermetallics* **1998**, *6*, 315–322. [CrossRef]
34. Calaway, M.J.; Fries, M.D. Adventitious Carbon on Primary Sample Containment Metal Surfaces. In Proceedings of the 46th Lunar and Planetary Science Conference, The Woodlands Waterway Marriott Hotel and Convention Center, The Woodlands, TX, USA, 16–20 March 2015; p. 1517.
35. Yoshitake, T.; Inokuchi, Y.; Yuri, A.; Nagayama, K. Direct epitaxial growth of semiconducting β-$FeSi_2$ thin films on Si(111) by facing targets direct-current sputtering. *Appl. Phys. Lett.* **2006**, *88*, 182104. [CrossRef]
36. Shaban, M.; Nomoto, K.; Izumi, S.; Yoshitake, T. n-type β-$FeSi_2$/intrinsic-si/p-type si heterojunction photodiodes for near-infrared light detection at room temperature. *Appl. Phys. Lett.* **2009**, *94*, 222113. [CrossRef]
37. Promros, N.; Baba, R.; Takahara, M.; Mostafa, T.M.; Sittimart, P.; Shaban, M.; Yoshitake, T. Epitaxial growth of β-$FeSi_2$ thin films on Si(111) substrates by radio frequency magnetron sputtering and their application to near-infrared photodetection. *Jpn. J. Appl. Phys.* **2016**, *55*, 06HC03. [CrossRef]
38. Abd Jelil, R. A Review of low-temperature plasma treatment of textile materials. *J. Mater. Sci.* **2015**, *50*, 5913–5943. [CrossRef]
39. He, L.P.; Cai, Z.B.; Peng, J.F.; Deng, W.L.; Li, Y.; Yang, L.Y.; Zhu, M.H. Effects of oxidation layer and roughness on the fretting wear behavior of copper under electrical contact. *Mater. Res. Express* **2020**, *6*, 1265e3. [CrossRef]
40. Junior, C.F.L.; de Assis Machado, G.S.; Mendes, P.S.N.; Huguenin, J.A.O.; Ferreira, E.A.; da Silva, L. Analysis of copper and zinc alloy surface by exposure to alcohol aqueous solutions and sugarcane liquor. *J. Mater. Res. Technol.* **2020**, *9*, 2545–2556. [CrossRef]
41. Lavieja, C.; Oriol, L.; Peña, J.I. Creation of superhydrophobic and superhydrophilic surfaces on ABS employing a nanosecond laser. *Materials* **2018**, *11*, 2547. [CrossRef]
42. Charoenyuenyao, P.; Promros, N.; Chaleawpong, R.; Borwornpornmetee, N.; Sittisart, P.; Tanaka, Y.; Yoshitake, T. Impact of annealing temperature and carbon doping on the wetting and surface morphology of semiconducting iron disilicide formed via radio frequency magnetron sputtering. *Thin Solid Films* **2020**, *709*, 138248. [CrossRef]
43. Quéré, D. wetting and roughness. *Annu. Rev. Mater. Res.* **2018**, *38*, 71–99. [CrossRef]
44. Wenzel, R.N. surface roughness and contact angle. *J. Phys. Chem.* **1949**, *53*, 1466–1467. [CrossRef]
45. Cassie, A.B.D.; Baxter, S. Wettability of porous surfaces. *J. Chem. Soc. Faraday Trans.* **1944**, *40*, 546–551. [CrossRef]
46. Fischer-Cripps, A.C. A review of analysis methods for sub-micron indentation testing. *Vacuum* **2000**, *58*, 569–585. [CrossRef]
47. Lu, C.J.; Bogy, D.B. The Effect of tip radius on nano-indentation hardness tests. *Int. J. Solids Struct.* **1995**, *32*, 1759–1770. [CrossRef]
48. Oliver, W.C.; Pharr, G.M. An improved technique for determining hardness and elastic modulus using load and displacement sensing indentation experiments. *J. Mater. Res.* **1992**, *7*, 1564–1583. [CrossRef]
49. Beegan, D.; Chowdhury, S.; Laugier, M.T. Comparison between nanoindentation and scratch test hardness (scratch hardness) values of copper thin films on oxidised silicon substrates. *Surf. Coat. Technol.* **2007**, *201*, 5804–5808. [CrossRef]
50. Murakami, T.; Hibi, Y.; Mano, H.; Matsuzaki, K.; Inui, H. Friction and wear properties of fe-si intermetallic compounds in ethyl alcohol. *Intermetallics* **2012**, *20*, 68–75. [CrossRef]
51. Chen, L.; Ahadi, A.; Zhou, J.; Ståhl, J.-E. Modeling effect of surface roughness on nanoindentation tests. *Procedia CIRP* **2013**, *8*, 334–339. [CrossRef]